Aerodynamics of Slender Bodies at High Angles of Attack

C.E.G. Przirembel*
Rutgers – The State University, Piscataway, N.J.
and
Donald E. Shereda†
Air Force Flight Dynamics Laboratory, Wright-Patterson Air Force Base, Ohio

Very high Reynolds number wind tunnel tests on models, which were approximately one-tenth of full-scale missiles, were conducted to investigate the significance of various pertinent test parameters. The test conditions were selected to insure turbulent flow prior to flow separation for the moderate to high angles of attack. Particular attention was focused on the relative importance of the roll angle on the measurement of the maximum side force. Mach number, Reynolds number, angle of attack, and the use of grit strips were other test variables considered in this analysis. It was concluded that in order to establish a reliable data base for the development of existing prediction methods, the roll angle must be varied by small increments for all wind tunnel tests.

Introduction

THE advent of missiles and supersonic aircraft, where the vehicle body is a major contributor to the overall aerodynamics of the system, has called for a major effort in understanding the problem of slender bodies of revolution at angles of attack. For instance, during the launch phase of an MX-class strategic missile from a large, high-performance transport aircraft, the missile is exposed to high subsonic/transonic flow at high angles of attack and at large freestream Reynolds numbers. Furthermore, the same flight environment exists during the launch of air-to-air missiles from strategic aircraft. Although in both cases the launch phase represents only a very short portion of the total missile flight time, the determination and control of strong side forces and moments is crucial to the completion of the desired mission.

Furthermore, the use of pointed fuselage forebody shapes for current supersonic aircraft has resulted in stability and control problems of these vehicles at high angles of attack. For extremely high angles of attack, such as those occurring during post-stall flight and spins, these vehicle geometries have been found[1] to produce large asymmetric yawing moments which can be significantly larger than the moments produced by the deflection of a conventional rudder. These moments alter the stall and spin characteristics to such an extent, that some recent losses of modern aircraft have been attributed to this problem.

In the range of angle of attack (α) from 0 to 90 deg, there are at least four distinct aerodynamic regimes. At very low angles of attack (regime I: $0 \leq \alpha \leq 5$ deg), there is no discernible boundary-layer separation, and the flow can be characterized by a classical potential flowfield and an attached laminar or turbulent boundary layer. As the angle of attack increases (regime II: $5 \leq \alpha \leq 20$ deg), the boundary layer begins to separate from the body, and the separated flow region moves forward with increasing angle of attack. The free shear layers roll up into two symmetric concentrated vortices, as shown in Fig. 1. These vortices are steady with time. For still higher angles of attack (regime III: $20 \leq \alpha \leq 70$ deg), the concentrated vortices break away from the slender body from alternate sides. This shedding process is periodic in a spatial sense, as shown in Fig. 2, rather than in a temporal sense as normally associated with the von Karman vortex street. These asymmetric vortices give rise to significant side forces and yawing moments. It is this flow regime, which is of primary interest in the current paper. Finally, as the angle of attack approaches 90 deg (regime IV: $70 \leq \alpha \leq 90$ deg), the flowfield is characterized by some form of temporal vortex shedding, as has been observed for infinite right circular cylinders. The appearance and disappearance of each regime as a function of angle of attack (α) is dependent on many factors, which include the nose shape, the overall fineness ratio, the cross-flow Mach number, and Reynolds number. Other factors may include roll angle, freestream turbulence, surface roughness, acoustic environment, and model/support system vibrations in wind tunnel studies. A critical review of the existing experimental data and prediction techniques for these flow regimes was reported by Przirembel.[2] Particular emphasis was placed on determining definitive trends in the variation of side forces and yawing moments in regime III.

The long-range objective of the current work is to predict the aerodynamic performance of full-scale systems. At the present time, there are no adequate theoretical prediction techniques, nor are there sufficient wind tunnel data that could be extrapolated with reasonable confidence to full-scale calculations. In an attempt to address the latter problem, a multiphase wind tunnel test program has been conducted to investigate the aerodynamic characteristics of advanced missiles for all four regimes, described earlier. Some of the data from this test program have undergone preliminary analyses, which have been reported by Baker and Reichenau,[3] Shereda and Dahlem,[4] and Deffenbaugh and Koerner.[5] The current paper reports results which were obtained for the largest physical wind tunnel model (about one-tenth of the anticipated full-scale system) and at the highest Reynolds numbers published in the open literature to this date. It has been previously established[2] that the side forces experienced by slender bodies at high angles of attack are influenced by small nose misalignment or by small surface irregularities. However, for much of the existing experimental data, the Reynolds numbers were in the transitional regime, and, by analogy with boundary-layer transition, the observed roll

Received Aug. 22, 1977; revision received July 5, 1978.

Index category: LV/M Aerodynamics.

*Associate Dean of Engineering, College of Engineering. Associate Fellow AIAA.

†Aerospace Engineer, High Speed Aero Performance Branch, Aero Mechanics Division.

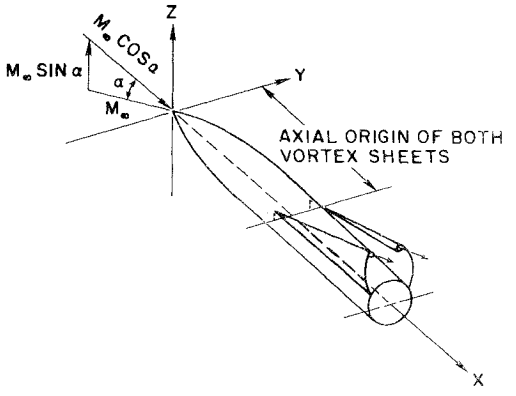

Fig. 1 Steady symmetric vortices ($5 \le \alpha \le 20$ deg).

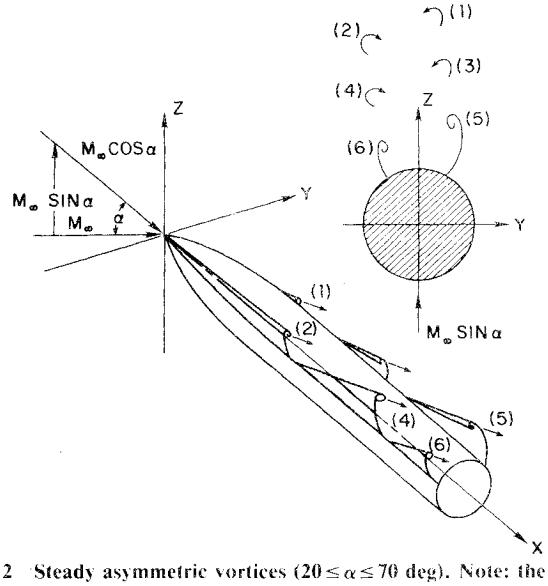

Fig. 2 Steady asymmetric vortices ($20 \le \alpha \le 70$ deg). Note: the axial origins of sheets 3 through 6 are all different.

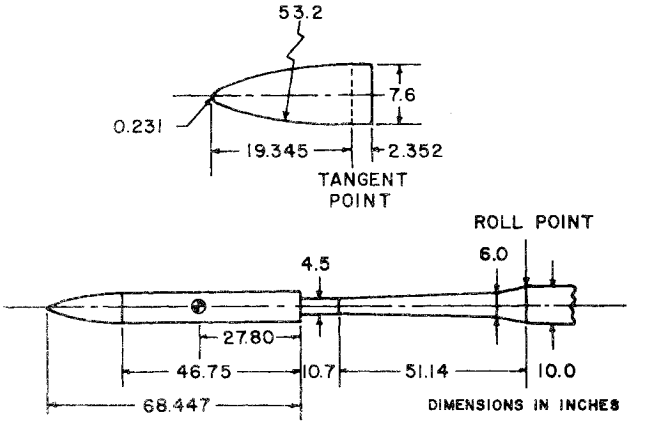

Fig. 3 Sting-mounted model with ogive nose.

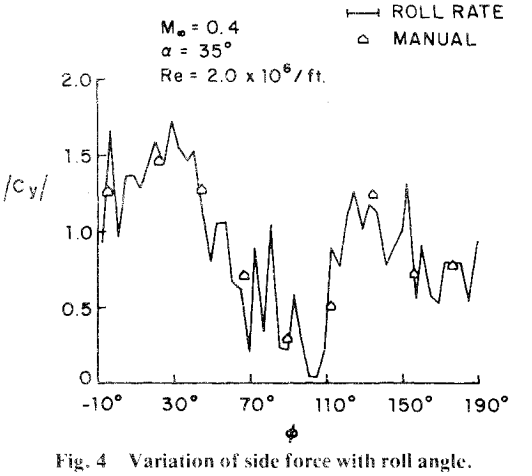

Fig. 4 Variation of side force with roll angle.

effects may have been caused by boundary-layer instabilities. One might then expect that the near full-scale or full-scale flow conditions are at sufficiently high Reynolds numbers that small geometric variations would not significantly affect the overall aerodynamics of the slender body. The current high-Reynolds-number results do not support this hypothesis and, in fact, underscore the difficulties in developing a reliable data base for designers.

Description of Experiment

The experimental investigations were conducted in the propulsion wind tunnel at the Arnold Engineering Development Center. This closed-circuit continuous-flow wind tunnel has a 16×16-ft test section, and is capable of operating within a Mach number range of 0.2 to 1.60 and a unit Reynolds number range of 0.50×10^6 to 6.0×10^6 per foot. The specific humidity of the air is controlled, and the stagnation temperature ranges between 80 to 160°F.

Figure 3 depicts the model and a portion of the sting support system. As shown, the most important, measurable geometric characteristics for this model were: 1) nose fineness ratio of 2.545, 2) nose bluntness ratio of 0.0304, and 3) cylindrical body length ratio of 6.461. These ratios are based on a cylindrical body diameter of 7.600 in.

The model was fabricated from 303 stainless steel with a number 32 finish. The above critical dimensions were kept within a tolerance of ±0.005 in. In some tests, a boundary-layer transition strip of No. 70 glass spheres was applied to the nose. Measured nose misalignment, which was determined by the nose mounting screws, was within ±0.009 in. This particular model represented an 8.59% scale model of an MX missile. Hence, the model tolerances were within the equivalent full-scale tolerances.

The model was mounted on a remotely controlled sting support system with a model angle of attack of −2 to 48 deg and a model roll range from −10 to 190 deg. Force measurements were obtained with a six-component strain-gage balance. These measurements were corrected for weight tares. Model angle of attack was measured with a strain-gage-type angle-positioning indicator, and the final value was corrected for balance and sting deflections. For tests with a roll angle, $\phi = 0$ the model was positioned at the specified angle of attack and the data were recorded with the model stationary. For two angles of attack ($\alpha = 35$, 40 deg), the model was normally rolled at a rate of approximately 2 deg/s. The roll point is shown in Fig. 3. Data were recorded at a rate of 100 samples per second on magnetic tape for off-line analysis.

The experimental investigation was conducted at freestream Mach numbers from 0.4 to 0.7 and at angles of attack from −2 to 48 deg. The freestream Reynolds number per foot varied from 0.5×10^6 to 5.0×10^6 at discrete Mach numbers.

Results and Discussion

A typical plot of the variation of the side-force coefficient (C_y) with roll angle (ϕ) is shown in Fig. 4. The individual data points were obtained in a separate test run, during which the model roll angle was set manually, rather than being rolled at a constant rate. The agreement between the two sets of data is reasonably good. Hence, for these conditions, data repeatability is good, and no apparent time-dependent flow switching seems to exist. Previous investigators[6-13] have commented primarily on the change of direction of the side

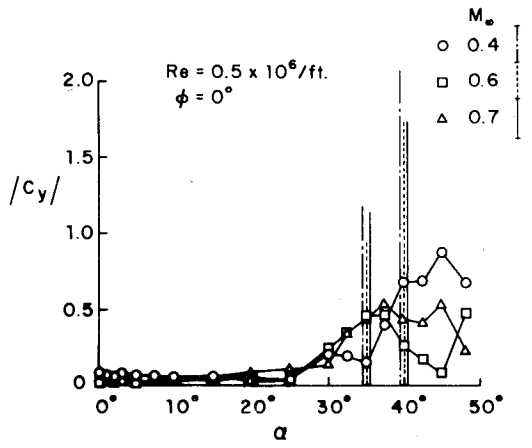

Fig. 5 Variation of side force with Mach number.

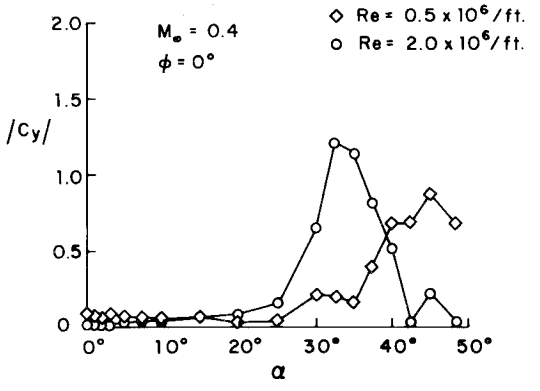

Fig. 6 Variation of side force with Reynolds number ($M_\infty = 0.4$).

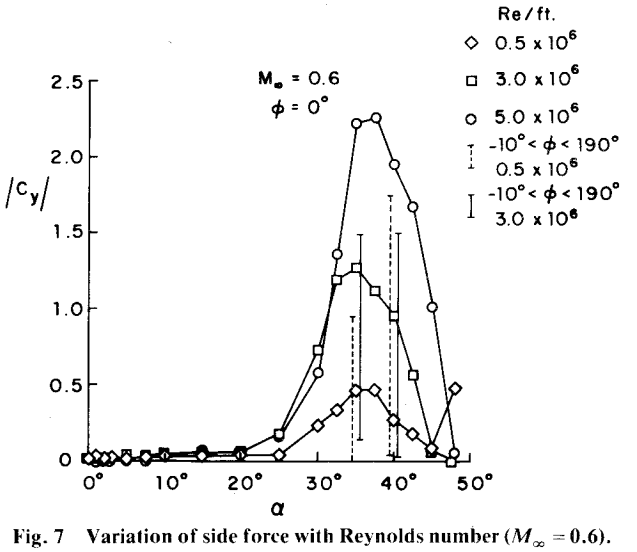

Fig. 7 Variation of side force with Reynolds number ($M_\infty = 0.6$).

forces, and not on changes in magnitude. Hence, in order to deliberately draw attention to the substantial changes in magnitude, the side-force data are presented in the form of absolute magnitudes. Figure 4 shows that the side force can change very rapidly with a small change in roll angle, and its magnitude is extremely dependent on roll angle. In contrast to the erratic behavior of the side force, the normal-force coefficient for this test varied from 3.0293 to 3.3948 over the roll-angle range. In comparing the relative significance of the side force to the normal force, it can be observed that the maximum side force is approximately 50% of the maximum normal force. Hence, the side force must be taken into consideration in the aerodynamic design of these missiles.

The variation of the side-force coefficient with the freestream Mach number is presented in Fig. 5. The Reynolds number and roll angle are constant. Concentrating first only on the data points plotted, it can be observed that the onset of significant side forces occurs for all Mach numbers at an angle of attack of about 25 deg. The Mach number effect is clearly ill-defined. At an angle of attack of 37.5 deg, the side forces seem to increase with the freestream Mach number; however, at an angle of attack of 48 deg, the trend is exactly in the opposite direction. Any apparent variations with Mach number are thoroughly overshadowed by the effect of roll angle on the data. For angles of attack of 35 and 40 deg, the three bar graphs show the maximum and minimum side forces measured by rolling the model continuously. Again, no distinct trends occur for these maximum values.

Figures 6 and 7 show the apparent increase of maximum side force (i.e., the local maximum value for each plotted curve) with Reynolds number. All plotted data points are for the same roll angle. At $M_\infty = 0.4$, the maximum side force seems to increase with increasing Reynolds number. The onset of significant side forces appears to be independent of Reynolds number. The angle of attack, at which the maximum side force occurs for a given roll angle, decreases with increasing Reynolds number. Due to the particular wind tunnel characteristics, 2.0×10^6 is the highest unit Reynolds number available for $M_\infty = 0.4$. As shown in Fig. 7, higher Reynolds numbers are obtained for $M_\infty = 0.6$. At this Mach number, there appears to be a very clear trend with Reynolds number, i.e., the local maximum side force increases with increasing Reynolds number. Up to this point, Figs. 6 and 7 have been analyzed in the usual manner, and reasonable trends appear to have been established. However, if the model is now rolled as indicated by the two bar graphs at $\alpha = 35$ and 40 deg, the apparent trends are no longer so conclusive. Again, the bar graphs show the maximum and minimum absolute values of the measured side forces. At $\alpha = 35$ deg, the maximum side force seems to increase with increasing Reynolds number. However, at $\alpha = 40$ deg, the trend is reversed. It was not possible to obtain roll data for the highest Reynolds number, because the model/support system vibrations became excessive. The cause of this stability problem was not determined, nor were any time-dependent force data measured. The current data were obtained at freestream Reynolds numbers, which were higher than for any previously reported investigations. However, these Reynolds numbers are still an order of magnitude lower than those encountered in the real flight environment.

Although most of the data presented in this paper and in the available literature[2] indicate that the maximum side force increases with increasing Reynolds number, some caution should be exercised in extrapolating side forces to full-scale models in the anticipated flight envelope. Obviously, the current roll data are too limited for us to draw any general conclusions from them.

The influence of a grit ring on the nose of the model seems to be Reynolds number dependent, as shown in Figs. 8 and 9. At the lower Reynolds number ($R_e = 2.0 \times 10^6$ per foot), the presence of a grit ring appears to increase the onset angle of attack and the magnitude of the maximum side force. At the higher Reynolds number, no significant difference between the two models is apparent. However, in view of the previously mentioned model/support system dynamics at this Reynolds number, the flowfield and the resulting forces may be completely dominated by the flow unsteadiness. Both figures indicate that the grit ring may cause a delay in the onset of significant side forces.

As it has been pointed out in the above discussion, the roll angle is a very important experimental parameter. In order to see this more explicitly, Fig. 10 shows the variation of side forces at various angles of attack with two discrete roll angles ($\phi = 0$, 30 deg). For these data, only the magnitude of the side force is consistently larger for $\alpha = 30$ deg. The basic side-force distribution curve does not seem to be changed. For com-

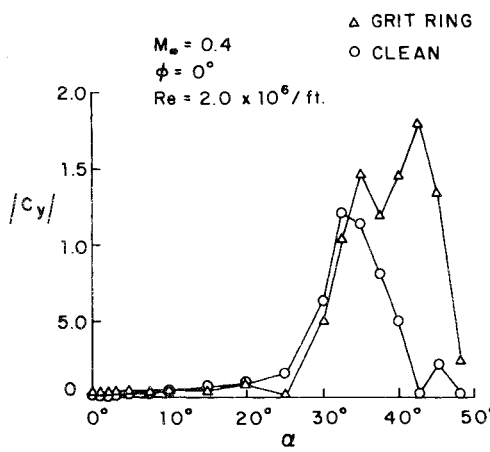

Fig. 8 Influence of nose grit ring on side forces ($M_\infty = 0.4$).

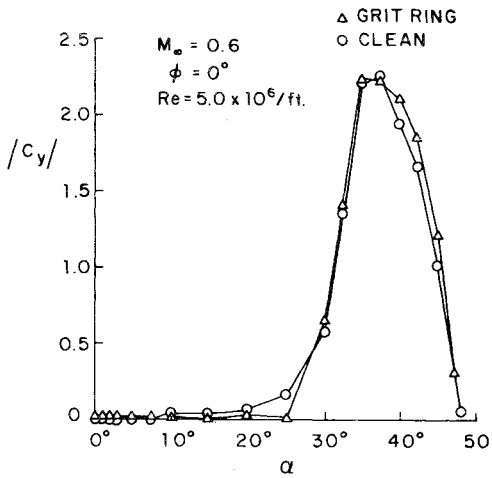

Fig. 9 Influence of nose grit ring on side forces ($M_\infty = 0.6$).

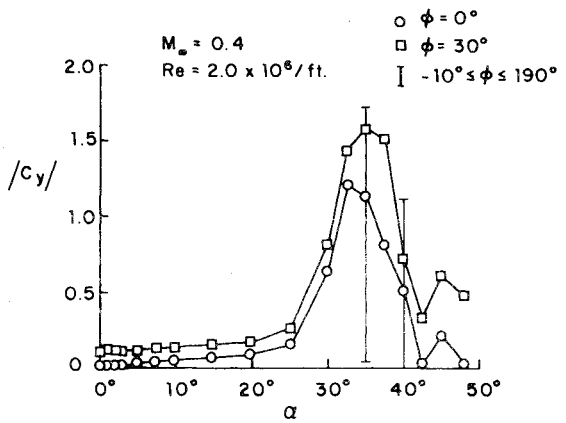

Fig. 10 Effect of discrete roll angles on side forces.

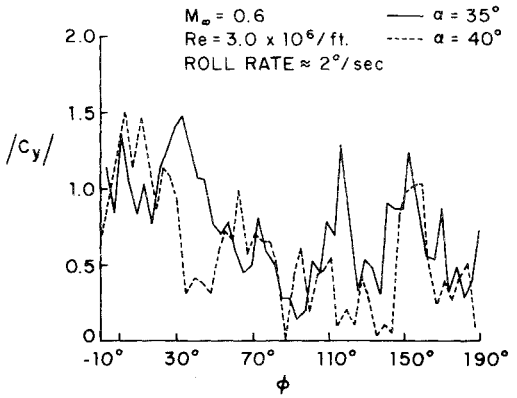

Fig. 11 Side-force distribution with roll angle.

parison with the continuously rolled data, two bar graphs are shown at $\alpha = 35$ and 40 deg. It appears that the maximum values follow the same general trend. For this particular case, the maximum values occurred at about the same roll angle. From an experimentalist's point of view, it would be very convenient if indeed the maximum side force for a particular model would occur at the same roll angle for various values of α, M_∞, and R_c. However, this does not seem to be necessarily true. In Fig. 11, the side-force variation with roll angles is shown for two different angles of attack. The maximum side forces occur at roll angles, which are approximately 30 deg apart. The general pattern of side-force variation with roll angle seems to be similar. These two results are consistent with the hypothesis that roll-angle effects are primarily a function of nose misalignment, and/or other irregularities in the construction of the model. Since these geometric nose variations are most likely three-dimensional in character, it appears reasonable to expect variations with angle of attack. Other factors, which might contribute to the variation of side forces, are the effect of flow unsteadiness and the characteristics of wind tunnel freestream turbulence. These effects have not yet been investigated.

Conclusions

This paper provides some limited, quantitative indication of the difficulties encountered in using wind tunnel data to predict the actual aerodynamic characteristics of slender bodies at moderate to high angles of attack. The experimental results were obtained for the largest physical wind tunnel model (about one-tenth of the anticipated full-scale system), and at the highest Reynolds numbers reported to date. In spite of the fact that the boundary layer approaching the separation line was turbulent, and therefore quite representative of full-scale flow conditions, very few definitive statements can be made about the variation of side forces with various experimental parameters. The apparently confusing and very often conflicting conclusions that have been drawn from existing data[2] can be attributed to the importance of such variables as roll angle and model support system dynamics, which are difficult to eliminate or even to control for a given wind tunnel model geometry.

In view of the current uncertainties in the available experimental data,[2] and in view of the utilization of numerous free-floating parameters in existing prediction techniques, any general conclusions drawn about the accuracy and usefulness of any one of the analytical techniques are not warranted at this time. It seems somewhat futile to exercise or attempt to improve the more elaborate multivortex models by adjusting the various constants to fit the results to a particular set of experimental data. For the purpose of design calculations, a linear regression model as proposed by Wardlaw and Morrison[14] may currently be the most practical approach. However, the available data base must be expanded by obtaining more extensive roll data and by minimizing the effect of some of the more esoteric experimental variables.

Acknowledgments

The authors gratefully acknowledge the fruitful discussions with J. Flaherty and V. Dahlem III, both of AFFDL. The senior author's work on this problem was initiated under the 1976 USAF-ASEE Summer Faculty Research Program (WPAFB). The current work was supported under AFOSR Grant 77-3300.

References

[1] Chambers, J.R., Anglin, E.L., and Bowman, J.S., Jr., "Effects of a Pointed Nose on Spin Characteristics of a Fighter Airplane Including Correlation with Theoretical Calculations," NASA TN D-5921, 1970.,

[2] Przirembel, C. E. G., "Aerodynamics of Slender Bodies at Angles of Attack – A Critical Review," High Speed Aero Performance Branch, Aeromechanics Division, Air Force Flight Dynamics Laboratory, AFFDSL-TM-76-92-FXG, Aug. 1976.

[3] Baker, D. C. and Reichenau, D. E. A., "Aerodynamic Characteristics of an MX Missile at Free-Stream Mach Numbers from 0.3 to 1.3 and Angles of Attack up to 180 Degrees," AEDC-TR-34, April 1975.

[4] Shereda, D. E. and Dahlem, V., III, "MX Missile Body-Alone Aerodynamic Characteristics at Mach Numbers 0.3 to 1.3 and Angles of Attack up to 180 Degrees," Air Force Systems Command, Wright-Patterson Air Force Base, Ohio, unpublished Rept. AFFDL/FXG, Oct. 1975.

[5] Deffenbaugh, F. D. and Koerner, W. G., "Asymmetric Wake Development and Associated Side Force on Missiles at High Angles of Attack," AIAA Paper 76-364; AIAA 9th Fluid and Plasma Dynamics Conference, San Diego, Calif.; also *Journal of Spacecraft and Rockets*, Vol. 14, March 1977, p. 155.

[6] Pick, G. S., "Investigation of Side Forces on Ogive-Cylinder Bodies at High Angles of Attack in the $M = 0.5$ to 1.1 Range," AIAA Paper 71-570, Palo Alto, Calif., June 1971.

[7] Coe, P. L., Jr., Chambers, J. R., and Letko, W., "Asymmetric Lateral-Directional Characteristics of Pointed Bodies of Revolution at High Angles of Attack," NASA TN D-7095, 1973.

[8] Keener, E. R. and Chapman, G. T., "Onset of Aerodynamic Side Forces at Zero Sideslip on Symmetric Forebodies at High Angles of Attack," AIAA Paper 74-770, Anaheim, Calif., Aug. 1974.

[9] Keener, E. R., Chapman, G. T., and Kruse, R. L., "Effects of Mach Number and Afterbody Length on Onset of Asymmetric Forces on Bodies at Zero Sideslip and High Angles of Attack," AIAA Paper 76-66, Washington, D.C., Jan. 1976.

[10] Lamont, P. J. and Hunt, B. L., "Pressure and Force Distribution on Sharp-Nosed Circular Cylinder at Large Angles of Inclination to a Uniform Subsonic Stream," *Journal of Fluid Mechanics*, Vol. 76, Aug. 1976, pp. 519-559.

[11] Lamont, P. J. and Hunt, B. L., "Prediction of Aerodynamic Out-of-Plane Forces on Ogive-Nosed Circular Cylinders," *Journal of Spacecraft and Rockets*, Vol. 14, Jan. 1977, pp. 38-43.

[12] Keener, E. R., Chapman, G. T., Cohen, L., and Taleghani, J., "Side Forces on a Tangent Ogive Forebody with a Fineness Ratio of 0.35 at High Angles of Attack and Mach Numbers from 0.1 to 0.7," NASA TM X-3437, Feb. 1977.

[13] Keener, E. R., Chapman, G. T., Cohen, L., and Taleghani, J., "Side Forces on Forebodies at High Angles of Attack and Mach Numbers from 0.1 to 0.7; Two Tangent Ogives, Paraboloid and Cone," NASA TM X-3438, Feb. 1977.

[14] Wardlaw, A. B., Jr. and Morrison, A. M., "Induced Side Forces at High Angles of Attack," *Journal of Spacecraft and Rockets*, Vol. 13, Oct. 1976, p. 589.